Issues in Stringing the CEBAF Large Acceptance Spectrometer Region 1 Drift Chamber: Pretensioning and Gravitational Sag

R.A. Thompson, S.A. Dytman, J.A. Mueller
University of Pittsburgh, Pittsburgh, PA 15260

October 10, 1996

Abstract

We present our solutions to two unusual problems encountered in stringing the CEBAF Large Acceptance Spectrometer Region 1 Drift Chamber (CLASR1): pretensioning and gravitational sag. It is shown that, because the endplates of CLASR1 are thin, it is important to address both of these issues. In order to devise a pretensioning scheme, we constructed an empirical model of the deflection of the endplate due to forces applied to it by wires. The details of this model are presented. The gravitational sag of the sectors of CLASR1 during construction was an important factor and the way in which we compensated for it is presented.

1 Introduction

CLASR1 is the inner drift chamber of CLAS. Details of the design are given in the Conceptual Design Report on CEBAF Basic Experimental Equipment [1]. CLASR1 is composed of six separate drift chambers (called sectors) as shown in Fig. 1. As with any large drift chamber, the construction of CLASR1 has presented many unique problems. Some of these challenges have come about because the long endplates of the sectors are not stiff to the scale of wire tensions. This lack of stiffness of the sectors lead to two important effects that required compensation.

First, the forces applied to the endplates by the detector wires causes the endplates to warp to such a degree that the tensions of wires are dramatically effected. We compensated for the deflection of the endplates by pretensioning the sectors prior to stringing. That is, we installed relatively few heavy steel wires in order to deform the endplates prior to stringing. The placement and loads of these pretension wires is not arbitrary. In order to understand how to pretension CLASR1, we constructed a mathematical model for the deformation of the endplates.

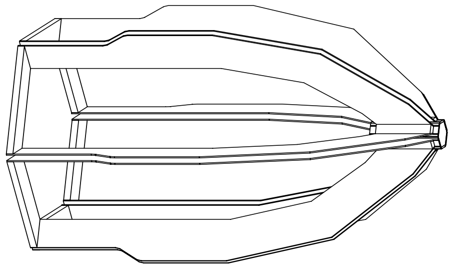

Figure 1: A drawing of CLASR1 showing the endplates, backplates, noseplates, and the hexagonal pipe that attaches the noseplates together. The posts that provide structural support before the sectors are integrated are not show. Each sector is assembled and strung seperately; it is only at the last stage that the six sectors are integrated.

Second, because the endplates are thin, the sectors sag due to gravity. This is an important factor in the tensions of the stereo angle wires. We dealt with the sag of the sectors by measuring its effect on the tensions of the stereo angle wires and simply compensating for it in stringing weights.

CLASR1 uses $140\mu m$ gold coated aluminum field shaping wires and $20\mu m$ gold coated tungsten sense wires. In compensating for the effects mentioned above, we wanted to keep the tensions on the field wires within 20g of the nominal 100g and the tensions on the sense wires to within 6g of the nominal 30g. These criteria determined the number of pretension wires, the number of pretension transfer steps, and the number of different sag compensation stringing weights we used. Since 90% of the entire load on the endplates is due to the field wires, we transfered the pretension load to the field wires first, then strung the sense wires. The effective spring constant of the sense wires is a factor of 9.2 less than that of field wires (eqns. 3), so for sense wires, the gravitational sag of sectors is not an important factor either. The warping and gravitational sag of the endplates are effects that are only relevant to the tensions on the field wires.

2 Pretensioning

The pretensioning of CLASR1 is presented. First, we present evidence showing that it was necessary to compensate for the warping of the endplates. We next outline a model used to understand the deformation of the surfaces of the endplates as a result of forces applied to them by wires. This model was used to choose the placement and load of the pretension wires. We also used this model to guide us in constructing a scheme to transfer tension from the pretension wires to the detector wires.

2.1 Motivation

This section describes the need for pretensioning the CLAS Region 1 drift chamber (CLASR1). The loss of wire tension due to the warping of the endplates is described and observations in a CLASR1 full scale prototype are presented.

The endplates of CLASR1 are constructed from plate aluminum 7.9mm in thickness. Each of the six sectors has 3435 field and guard wires strung at a nominal tension of 100g and 1296 sense wires strung at a nominal tension of 30 g for a total of 3.75 kN (843 lbs) of force on each endplate. The endplates will deform as a result of this heavy load and the surface of the endplates will no longer be flat. As the sector is strung, the wires that were strung earlier will lose tension because the wires that were strung later will pull the endplates together. Fig. 2 shows this effect after stringing about 12% of a full-scale prototype sector.

Based on measurements of this endplate deformation in the prototype and a model that will be presented later in this paper, we anticipated that if we did not compensate for this phenomenon in a sector where 100% of the detector wires are strung, some wires would go completely slack. For a wire with some tension applied to it such that Hooke's law is applicable, a change in length ΔL of a wire of length L will lead to a change in effective mass Δm (the effective mass is just $m = T/g$, where g is the acceleration due to gravity) according to

$$\Delta m = k \cdot \frac{\Delta L}{L} \tag{1}$$

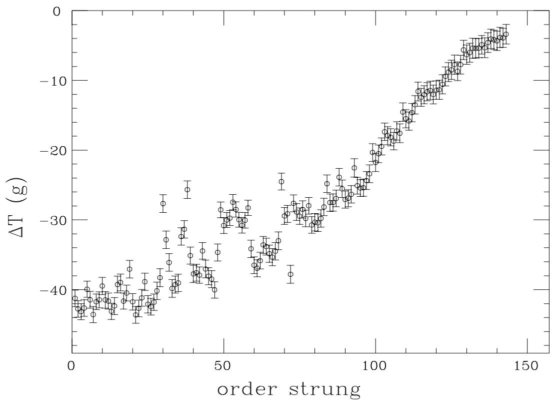

Figure 2: The tension change on tension monitoring wires strung in the full scale CLASR1 prototype plotted versus the order that those wires were strung. The tension monitoring wires that were strung first lost tension as a result of the wires that were strung later. Since only a small section of the prototype was strung, this effect would be much worse in the real detector if there were no pretensioning.

The constant k is given by

$$k = \frac{Y \cdot A}{g} \tag{2}$$

where Y is Young's modulus and A is the cross sectional are of the wire. We measured Young's modulus for the $140\mu m$ gold coated aluminum field wire, and for the $20\mu m$ gold coated sense wire and obtained

$$\begin{aligned} k_{field} &= 1.10 \cdot 10^5 \; grams \\ k_{sense} &= 1.19 \cdot 10^4 \; grams \end{aligned} \tag{3}$$

We predicted that due to the deformation of the endplate, the length of some wires in the sectors would change by as much as 0.064cm, which corresponds to 105g by eqn. 1. This length change is certainly outside of the range where the wire will obey Hooke's law, but the conclusion that these wires will go slack is still valid.

The observation of wire tension loss due to endplate deformation in the CLASR1 full scale prototype and our predictions of the scale of the effect in the actual detector indicated a real need for pretensioning. The objectives of pretensioning are twofold. First, the pretensioning should mock the deflection of the endplates with relatively few pretensioning wires that are installed prior to stringing. And second, the tension in the pretension wires should be transfered to the detector wire in such a way that the final tensions on the detector wires are within an acceptable range of nominal. Both of these objectives necessitate some quantitative understanding of how the surface of the endplate is deflected as a result of the forces applied to it by wires. We felt that a model describing the surface of the endplate would be a more efficient approach than an exact solution derived from the complicated boundary conditions and the material properties of the endplate.

2.2 A Model for Endplate Deflection

Fig. 3 shows the geometry of the problem. All points are referenced to a coordinate system that is on the flat surface of one endplate. An arbitrary origin is chosen. We determine the deflection of the endplate from flatness, $D(\vec{x})$, at the point $\vec{x}$ due to the force T exerted on the endplate by the wire located at $\vec{p}$. Posts are located at the points described by $\vec{h}_i$. The point $\vec{x}$ is located along a ray originating from the wire. The direction of this ray is described by the unit vector $\hat{r}$ as shown.

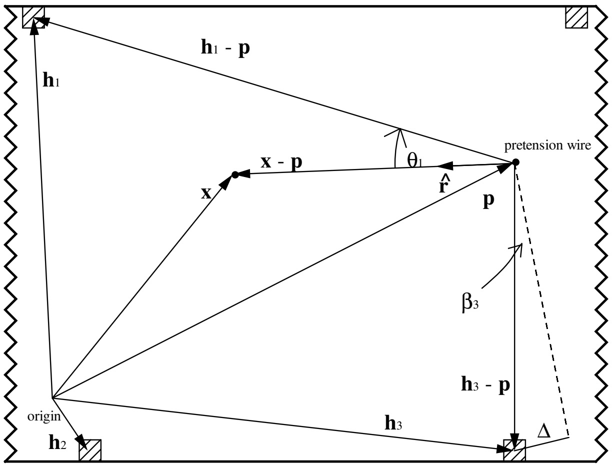

Figure 3: A schematic drawing defining the geometry on the surface of an endplate. The border of the endplate, which continues to the left and right, is shown as a bold line. Posts are indicated by hatched squares and are located at the points given by $\vec{h}_i$. A wire (detector wire or pretension wire) is located at the point $\vec{p}$ and the point at which the endplate deflection is being considered is given by the point $\vec{x}$.

Our approach was to use intuitive physical principles to construct a model which describes the deflection of the endplate due to the forces applied to it by wires. The model contains some parameters which could then be fit by taking measurements of endplate deflections. There are two general assumptions we used to choose a form for $D(\vec{x})$: 1) The magnitude of the deflection of the endplate at the location of the wire is proportional to the tension in that wire. 2) The shape of the endplate along polar rays centered at the wire is a straight line. With these assumptions, the deflection of the endplate is written

$$D(\vec{x}) = T \cdot [m(\theta) \cdot |\vec{p} - \vec{x}| + K(\vec{p})] \tag{4}$$

Here $m(\theta)$ is the slope of the endplate along a ray centered at the wire, θ is the polar angle of the ray, and $T \cdot K(\vec{p})$ is the deflection of the endplate at the location of the pretension wire. It is $m(\theta)$ that describes the wrinkles forced in the endplate by posts.

As can be seen from eqn. 4, the ideas of the model presented here are very simple. The geometry of the problem, though, makes the implementation of the model more complicated. Specifically, the model must be able to accomodate boundary conditions of zero deflection at various locations. The endplates are fastened at the upstream and downstream ends to rigid plates, and during construction, the endplates are fastened to each other by 22 rigid posts. At these points, the deflection of the endplates is constrained to be zero. As Fig. 4 shows, the location of these boundary conditions (and also the shape of the endplates) is in no way simple.

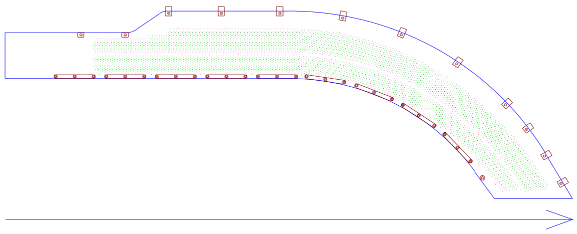

Figure 4: The surface of an endplate. The beam axis and direction are indicated by the arrow. The length of the endplate along the beam axis is 2.28m. The shaded region is where the detector wires are strung in two superlayers: one with wires perpendicular to the beam axis and one with wires tilted at a 6° angle relative to the beam axis. The posts along the top edge are located where the rectangular mounting brackets are shown. The posts along the bottom edge are located at the center of the long mounting brackets. The deflection of the endplate is constrained to be zero at the location of posts and where the endplate attaches to rigid plates at the upstream (left) vertical edge and the downstream horizontal edge. The geometry of these constraints makes for a complex set of boundary conditions that a model of endplate deflection must obey.

The model can conceptually be broken down into two aspects: 1) $K(\vec{p})$, the magnitude of the deflection of the endplate at the location of the wire and the dependence of this deflection on the proximity to posts and rigid edges, 2) $m(\theta)$, the shape of the endplate along polar rays originating at the wire and the dependence of the shape of these rays on the polar angle.

2.2.1 Deflection at the Wire: Flexibility

Let $S(\vec{p})$ be the deflection of the endplate from flatness at the location of a wire. $S(\vec{p})$ should depend on two things: the tension in that wire and the distance of that wire from the rigid constraints of plates and posts. Asalready mentioned, we assumed that the deflection of the endplate at a wire is proportional to the tension in that wire: $S(\vec{p}) = T \cdot K(\vec{p})$. Fig. 5 shows that for tensions less that 133N (30lbs), this is indeed the case.

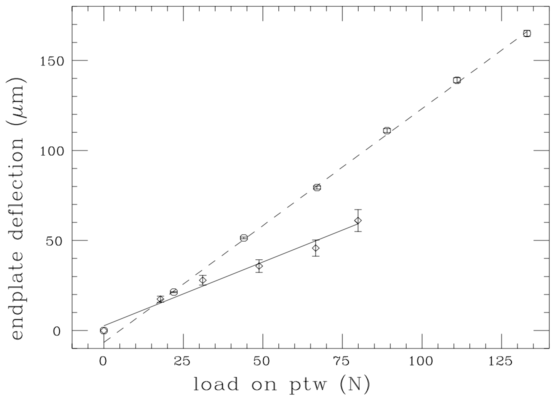

Figure 5: The deflection of the endplate at the positions of two wires plotted as a function of the loads on the wires. Since these two wires are at different locations on the endplate, the slopes of the two lines should not necesarily be the same. The slope of the line is $K(\vec{p})$. The wire represented by the diamond symbols and the solid line was located at a more rigid place in the sector than was the wire represented by the circular symbols and dashed line.

$K(\vec{p})$ is a measure of the flexibility of the endplate and should depend on the location of the wire relative to posts and rigid edges. $K(\vec{p})$ is subjected to two limits: 1) The endplates are rigid at posts, $K(\vec{h_i}) = 0$. 2) The flexibility of the endplates approaches some asymptotic value far from posts or rigid edges. We chose a gaussian as the mathematical form for the transition between these two limits. For a single post, we write the flexibility of the endplate as

$$K_i(\vec{p}) = K_0 \cdot \left(1 - e^{-\frac{1}{2\alpha^2}\left|\vec{p}-\vec{h_i}\right|^2}\right). \quad (5)$$

K_0 is the asymptotic value of the flexibility; its value for an infinite sheet of material. α is a parameter which describes the dependence of the flexibility on the proximity to posts and rigid edges. Multiple posts and rigid edges are accomodated by including a factor of $(1 - e^{-\frac{1}{2\alpha^2}\left|\vec{p}-\vec{h_i}\right|^2})$ for each post:

$$K(\vec{p}) = A \cdot \prod_i \left(1 - e^{-\frac{1}{2\alpha^2}\left|\vec{p}-\vec{h_i}\right|^2}\right). \quad (6)$$

Fig. 6 shows the flexibility for a simple hypothetical endplate. A and α are parameters that are fit to measurements of endplate deflection.

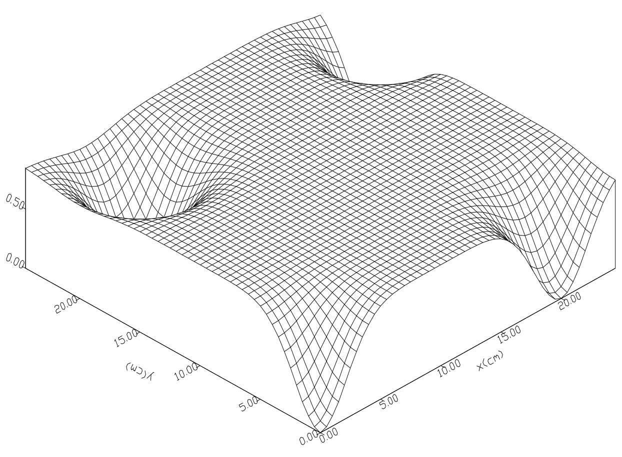

Figure 6: The flexibility of the enplate (in units of $\mu m/N$) plotted over the surface of a hypothetical endplate. Posts are located where the flexibility goes to zero.

2.2.2 Shape Along Polar Rays

We assumed that the surface of the endplate along polar rays centered at the wire under consideration is straight. By taking endplate deflection measurements, we demonstrated that this is the case for wire tensions less than 133N (30lbs), as shown in Fig. 7. The slope of the endplate along these rays is $m(\theta)$ from eqn. 4.

Consider the simple case where there is only one post. Let $m_i(\theta)$ be the contribution to the slope of the endplate along the ray $\hat{r}$ due to that post. $m_i(\theta)$ has two limits, similiar to $K(\vec{p})$. 1) When the ray from the wire points to a post $\left(\hat{r} = \frac{\vec{p}-\vec{h_i}}{\left|\vec{p}-\vec{h_i}\right|}\right)$, $m_i(\theta)$ is determined from $S(\vec{p})$ and the distance from the wire to the post $\left|\vec{p} - \vec{h_i}\right|$. Let θ_i be the polar angle from the wire to the i_{th} post. Then

$$m_i(\theta_i) = -\frac{S(\vec{p})}{\left|\vec{p} - \vec{h_i}\right|} \quad (7)$$

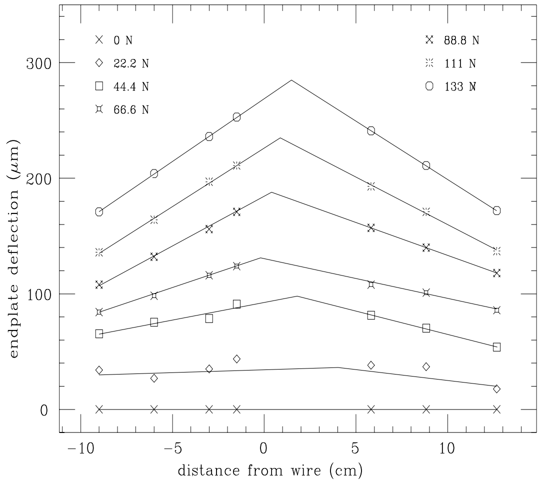

Figure 7: Deflection of the endplate as a function of distance from the wire for various loads. This essentially shows cross sections of the surface of the endplate with different loads applied to a wire. The distance from the wire is along a particular polar ray from the wire. The solid line is the shape of the deflected endplate that we infer assuming a linear shape along polar rays.

2) When $\hat{r}$ points in a direction far from any posts, $m_i(\theta)$ should approach some asymptotic value. We assume that the form of the transition between these two limits is gaussian:

$$m_i(\theta) = p_0 + p_i \cdot e^{-\frac{1}{2\beta_i^2}(\theta-\theta_i)^2} \tag{8}$$

Here p_0 is the asymptotic value that $m(\theta)$ takes when $\hat{r}$ points away from any posts. For an infinite sheet of material, p_0 is the slope of the surface of the material along a ray centered at a wire that has one unit of tension applied to it. β_i is the angular width of the gaussian wrinkle formed by a post. β_i depends on the distance between the wire and the post, but can be related, as shown in Fig. 3, to a parameter Δ which represents in some sense the stiffness of the material (similiar to α).

$$\beta_i = cos^{-1}\left(\frac{2\left|\vec{p}-\vec{h}_i\right|^2 - \Delta^2}{2\left|\vec{p}-\vec{h}_i\right|^2}\right) \tag{9}$$

Of course, in reality there are many posts. We accomodate multiple posts by including a term of Eqn. 8 for each post:

$$m(\theta) = p_0 + \sum_i p_i \cdot e^{-\frac{1}{2\beta_i^2}(\theta-\theta_i)^2} \tag{10}$$

In this equation, the p_i are treated as n unknowns (n is the number of posts being considered), but there are also n equations from which to determine the value of the p_i: when θ is such that the polar ray from the wire points at one of the posts, the value of $m(\theta)$ is known from eqn. 7.

With the flexibility $K(\vec{p})$ given by eqn. 6, and the wrinkle shape $m(\theta)$ given by eqn. 10, the endplate deflection is completely determined by eqn. 4. Fig. 8 shows the endplate deflection for a hypothetical endplate.

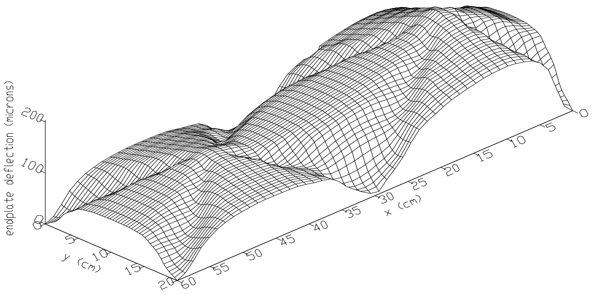

Figure 8: The surface of an endplate with six posts located at (0,0), (30,0), (60,0), (60,20), (30,20), and (0,20), and two wires located at (10.5, 10.5) and (45.5,10.5) with loads of 111N and 66.6N respectively.

We introduced four parameters during the construction of the model. These parameters were fit to measurements of endplate deflection. The values determined for them are:

$$\begin{array}{rcl} K_0 & = & 2.16\ \mu m\ N^{-1} \\ \alpha & = & 2.21\ cm \\ \Delta & = & 2.19\ cm \\ p_0 & = & 0.111\ \mu m\ cm^{-1} \end{array} \tag{11}$$

2.3 Pretensioning Scheme

With a model for endplate deflection in place, a scheme for pretensioning CLASR1 could be considered. We used the model to determine the correct number, location, and load for the pretension wires. We also modelled the transfer of tension from the pretension wires to the field wires.

In choosing the pretension wires, we wanted to keep the tension change on wires to less than 10 grams, while using as few as possible pretension wires. We first calculated the deflection of the endplate with all of the detector wires. This represents the "strung" shape of the surface of the endplate if all wires were installed at nominal tensions. We next carried out an analogous calculation of endplate deflection with pretension wires and varied the number, location, and load of pretension wires until the difference between the "pretensioned" and "strung" endplate surfaces was such that the corresponding change in wire tensions was less that 10g. Our final pretensioning consisted of 67 wires with effective mass loads ranging from 2 to 14 kg.

Next, we considered how to transfer the tension from the pretension wires to the detector wires. When the load in a pretension wire is reduced, the detector wires that have been installed to that point will become tighter. The detector wire installed immediately before a pretension transfer is then tighter than the detector wire installed immediately after a pretension transfer. A second objective in working out a pretension transfer procedure was to keep this tension difference between certain adjacent wires to less than 10g. The issue then is the number of pretension transfers performed on each pretension wire, and the point in stringing that each pretension transfer is performed. For the sake of expedience in stringing the sectors, we wanted to have no more than three tension transfers performed on each pretension wire.

We determined a scenario for pretension transfer by calculating endplate deflections for each pretension wire individually. We determined that we could perform three or fewer pretension transers, each of equal tension change and with an equal number of detector wires strung between each, and stay within the specification mentioned above.

3 Gravitational Sag

The CLASR1 sectors were strung on their sides (beam axis horizontal) so that the wire could be lowered through the feedthroughs in both endplates. During construction, each sector was mounted on a stringing frame and attached to it at the nose and back plates. The frames allow the sector to be oriented at any azimuthal angle. The sector azimuthal angle is here defined as the angle of the midplane between the two endplates as one would see it looking from upstream. 9 o'clock is then the orientation of the sector where the midplane between the endplates is parallel to the floor and to the left as seen from upstream. The sectors were strung in the 9 o'clock orientation.

Stringing the sectors at the 9 o'clock orientation facilitated installation of the wires, but allowed the sector to sag, as they were mounted to the stringing frame only at the nose and back. When a sector is oriented such that the surfaces of the endplates are nearly parallel with the ground (the surfaces of the endplates are mounted 30° to eachother), they bow down due to their own weight. But when a sector is oriented such that the surfaces of the endplates are nearly perpendicular to the ground, the sectors are stiff in the direction that the force of gravity is acting, and there is no sag. We verified that wire tensions in the 6 or 12 o'clock orientations best matched those of a sector that was not mounted to a stringing frame and not subjected to gravitational sag. In the 3 o'clock or 9 o'clock orientations, each of the sectors sagged by about 6mm at the middle. As illustrated in Fig. 9, this will cause the stereo super layer wires at the nose to be shorter, and the wires at the back to be longer, relative to the 12 o'clock or 6 o'clock orientations, where the sectors do not sag. The tensions in the axial super layer wires will be unaffected by the gravitational sag of the sector.

We determined the effect of the gravitational sag of the sectors by measuring wire tensions at 9 o'clock (where the sectors are strung) and at 12 o'clock. This allowed us to compensate for the sagging of the sector by adjusting nominal stringing tensions along the length of the sector. As Fig. 10 shows, the sector sag effect is dramatic.

The sense wires we used are about nine times less sensitive in tension to length changes (see eqns. 3). Because of this, we did not compensate for gravitational sag while stringing the stereo angle sense wire.

4 Results

Having described the issues of pretensioning and gravitational sag and the techniques we developed to deal with them in sections 2 and 3, we shall in this section present the final tensions of wires in the first three sectors that resulted from our solutions to these problems.

4.1 Pretensioning

The final tensions of the axial wires are dominated by pretensioning effects since the gravitational sag of the sectors does not affect those wires. The final tensions of the axial wires is then a measure of our solution to the problem of pretensioning.

Fig. 11 shows the final tensions of the axial field and guard wires for sector 1. This was our first attempt at implementing the endplate deflection model and pretension transfer scheme discussed previously. There are thirty boundary conditions of zero deflection imposed by posts and rigid edges. In order to simplify the realization of the model in code, we divided the sector up into nine sections, each bounded by four posts. By the time sector 1 was strung, we

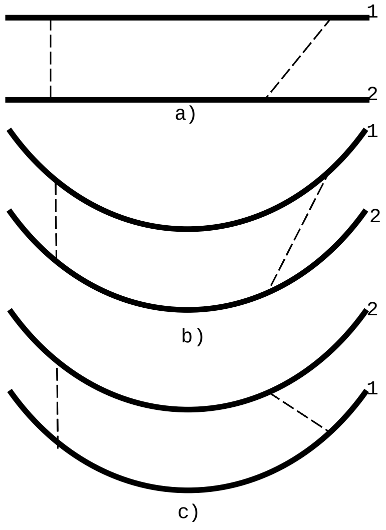

Figure 9: An illustration of two plates supported at the ends and the effect of gravitational sag on wires strung between the plates. The drawings show cross sections of two plates (bold lines) with two wires (dashed lines) strung between them. The wire that is perpendicular to the plates is analogous to an axial wire and the wire that is not normal to the plates is analogous to a stereo angle wire. The plates are numbered 1 and 2 in order to reference the stereo angle. The configuration of the plates and wires without gravitational sag is shown in Fig. (a). An exaggerated gravitational sag is shown in Fig.(b), where the lengthening of the stereo angle wire is evident. Fig. (c) shows the situation where the plates have been flipped over (plate 2 is on top) and the stereo angle wire is shortened. To first order, the length of the axial wire is unaffected by gravitational sag.

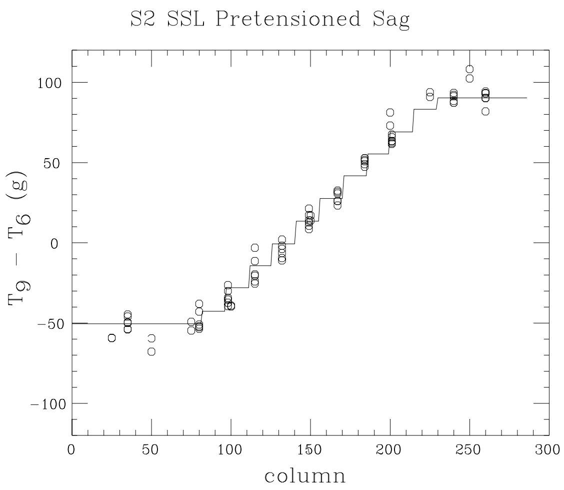

Figure 10: The change in stereo super layer field wire tensions resulting from the gravitational sag of sectors plotted versus the wire column. This test indicated that wires in the nose of the sector gain 50g of tension and the wires in the rear of the sector lose 90g of tension as a result of the sector being rotated from 9 o'clock (stringing position) to 6 o'clock (sag-free position). The circles show the results of the test that was repeated a number of times and the line shows the curve that we used to compensate the stringing tensions.

had coded the model so that all 30 boundary conditions could be simultaneously satisfied. Based on the sector 1 final tensions show in Fig. 11, we also globally increased the pretensioning for sector 2 by 10%.

For sector 2, we determined the pretensioning from the improved calculation that imposed all boundary conditions simultaneously. This allowed us to calculate the endplate deflection for the entire sector with all 4731 detector wires or with all of the pretension wires. Fig 12 shows the final tensions on the axial super layer wires of sector 2 and represents a significant improvement over those of sector 1 as shown in Fig. 11. The sawtooth shaped variation of the tensions along the sector is an effect due to pretensioning.

In stringing sector 3, we wanted to have two crews stringing the axial super layer at one time. This necessitated redetermining the pretension transfer scheme for nose to rear stringing (nose is defined as column 1). We had one crew working in the nose stringing towards the rear and one crew working in the rear working towards the nose. The two crews met in sector 3 at column 127. Then the pretension transfer in the rear of sector 3 (columns 127 through 286) was the same as it was in sector 2, while the pretension transfer for the nose of sector 3 was changed for the nose to rear stringing. The point where the two crews met is also evident by the spike near column 127 in Fig. 13. This came about because it was not possible to match the two pretension transfer schemes (nose to rear and rear to nose) without knowing ahead of time where the two crews would meet. As a result of this, 20 wires were restrung on sector 3.

The pretensioning for sectors 4 through 6 will be based on that of sector 3, perhaps with minor changes to flatten some of the larger variations.

4.2 Gravitational Sag

As previously mentioned, we chose to deal with the gravitational sag of the sectors during stringing by compensating for it in the nominal stringing tensions. The objective here was to string the stereo super layer

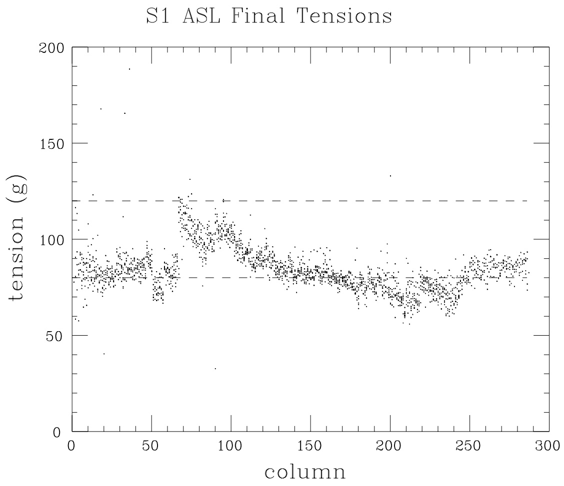

Figure 11: The final tensions of the field and guard wires in the sector 1 axial super layer. The wire tensions are plotted versus wire column, which is essentially the distance along endplate. Column 1 is defined as the upstream end of the sectors (the nose). The pretensioning and the pretension transfer scheme used on sector 1 were based on a simplified model that divided the sector up into nine sections bounded by posts, and calculated the endplate deflection with only the boundary conditions of those four posts imposed. The wires whose tensions lie far from the main band either had an incorrect tension monitoring reading taken or were restrung. This is true for all of the final wire tension plots shown in this paper.

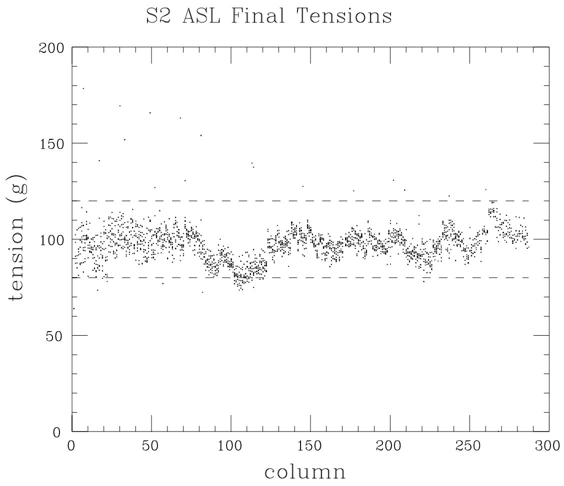

Figure 12: The final tensions of the field and guard wires in the sector 2 axial super layer. The pretensioning for sector 2 was determined using a model that solved the endplate deflection for an entire sector simultaneouly.

field wires at whatever tension was necessary such that when the sector was oriented at 12 o'clock or 6 o'clock the field wire tensions were $110 \pm 20g$. We strung stereo super layer field wires at tensions T_{string} which was adjusted from the nominal tension T_{nom} ($110g$) by an amount ΔT, which is the amount by which the tension is expected to change when the sector is oriented at 12 o'clock. T_{string} varies along the length of the endplate.

$$T_{string} = T_{nom} + \Delta T \qquad (12)$$

Prior to stringing sector 2 (but after it was pretensioned), we measured ΔT by measuring the tension in a set of wires when the sector was oriented at 9 o'clock and when it was oriented at 12 o'clock. Then $\Delta T = T_9 - T_{12}$. Fig. 10 shows ΔT as measured in a fully pretensioned sector 2. As shown in that figure, we used 12 different stringing weights to string the stereo super layer of sector 2 ranging from 50g to 190g.

Since the endplates are rigidly fastened to a plate at the nose of the sectors, the gravitational sag of the sector must be zero there. Then the solid line in Fig. 10 must return to 0g at column 0. Fig. 14 and Fig. 15 show measurements of ΔT taken after all detector wires were installed in sector 2 and 3 respectively, and clearly show this effect. Unfortunately, these measurements also indicate that the gravitational sag of sectors is different when the detector wires are installed and is different from sector to sector. The difference in the sag between sectors 2 and 3 was in the region from columns 20 to 50. In this region, the stereo field wires in sector 2 became much tighter at 12 o'clock than did those in sector 3. The sag compensation stringing weights for sector 3 were based on the solid line shown in Fig. 14.

The sag compensation stringing tensions used for sector 3 are given in Table 4.2. The final tensions on the sector 3 stereo super layer wires are show in Fig. 16. The difference between the gravitational sag of sectors 2 and 3 is evident from this plot. If the gravitational sag of sectors 2 and 3 had been the same, then the sag compensation used on sector 3, which was based on measurements of the sag of sector 2 (Fig. 15) would have been correct and the data points in Fig 16 would follow the solid line. Instead, it can be seen that the tensions in the wires in the rear of sector 3 changed by 10 - 20g less than was expected, and the tensions on the wires in the nose of sector 3 changed by 20 - 30g less than was expected. Based on these observations, the sag compensation for sectors 4 through 6 will be measured on those sectors (instead of on a previously strung sector) after the axial wires are strung, but before the stereo wires

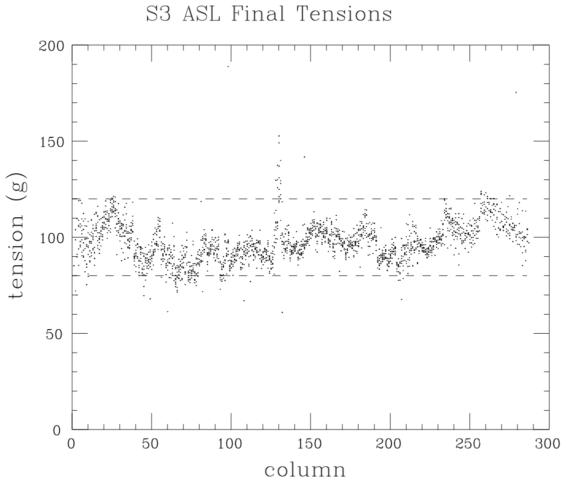

Figure 13: The final tensions of the field and guard wires in the sector 2 axial super layer. The pretensioning was the same as that of sector 2 except that the columns 1-127 of sector 3 were strung from nose to rear whereas all of sectors 1 and 2 were strung from rear to nose. The spike around column 127 is the point that the two crews stringing sector 3 in different directions met in the middle. At that point the pretension transfer schemes did not match up.

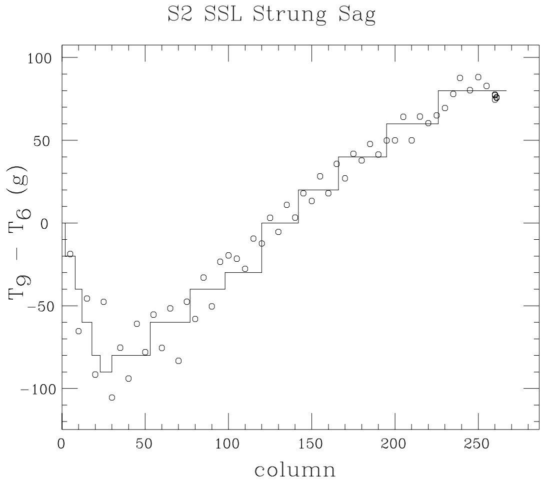

Figure 14: The sag effect in sector 2 after all of the detector wires had been installed. The circles show the measurements and the solid line shows the compensation curve that was used to string sector 3. That $T_9 - T_{12}$ goes to 0g at column 0 is necesitated by the fact that the endplates are rigidly fastened to a plate there. The same effect is not observed in the rear of the sectors because the wires there are far from the rear rigid fastening plate as can be seen from 4. The dip between columns 20 and 50, which indicates that these wires were 80 - 90g tighter at 6 o'clock than at 9 o'clock, was not observed in any of the other sectors.

are strung. There must be some pretensioning in the stereo super layer while the axial super layer is being strung, but the exact stringing tensions for the sector 4 stereo super layer are not known until the sector 4 sag effect is measured after the axial super layer wires are strung. In order to establish some pretensioning in the sector 4 stereo super layer that would be very close to correct, we used the stringing weights based on the sag effect from sector 3 (Fig. 15). It is not expected that the gravitational sag of sector 4 will be dramatically different from that of sector 3.

Then it is clear that the sag compensation for a sector cannot be based on measurements from another sector, or on measurements from that sector with no load or pretension wires only. For sectors 4 through 6, we will base the sag compensation on a measurement made on those sectors after the axial super layer field and guard wires are strung, but before the stereo super layer wires are strung. But before any stringing can take place, there must be pretensioning in both super layers, so we will use the sag measurement shown in Fig. 15 to determine the stereo super layer pretensioning. The pretensioning in the stereo super layers of these sectors will then not correspond to the stringing tensions of the actual wires. We would then need to change the stereo super layer pretensioning in the nose after the axial super layer have been strung. We have determined that this will typically cause as much as a 10 g change in some axial wires, but this is certainly much less that the 40g change in some stereo wires when the gravitational sag is not done properly, as shown in Fig. 16.

5 Summary

We have presented in detail our technique for dealing with two problems that arose in stringing CLASR1: pretensioning and gravitational sag. Both of these problems exist because the endplates of CLASR1 are by necessity thin. Measurements taken on the deflection of the endplates as a result of forces applied to them by wires indicated that if we did not pretension the sectors prior to stringing, some wires would go slack. The gravitational sag of the sectors in the stringing position also had a dramatic effect on the tensions of the stereo angle field and guard wires, making the aluminum wires in the nose 50 too tight and those in the rear 90 g too loose.

For pretensioning, our objective was to keep the field and guard wire tensions with in 20 g of 100 g. It can be seen in Fig. 13 that this goal was realized.

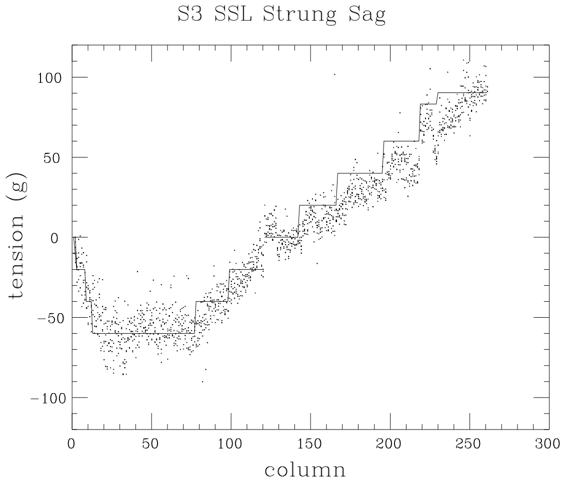

Figure 15: The gravitational sag in sector 3 after all of the detector wires had been installed. The solid line shows the sag compensation stringing tensions that was used to establish the pretensioning for sector 4.

Columns	Nominal Stringing Tension (g)
1 - 2	100
3 - 8	80
9 - 12	60
13 - 18	40
19 - 23	20
24 - 30	10
31 - 53	20
54 - 77	40
78 - 98	60
99 -120	80
121 -142	100
143 -166	120
167 -195	140
196 -226	160
227 -267	180

Table 1: The nominal field and guard wire tensions for the stereo super layer of sector 3. This gravitational sag compensation was arrived at by taking measurements of the sector 2 gravitational sag after it was completely strung (see Fig. 14)

We believe then, that the endplate deflection model was accurate for these purposes.

Our ability to control variations in the stereo angle aluminum wires was limited by the fact that this effect is apparently different for each sector, and different depending on wether pretension or detector wires are installed. Fig. 16 illustrates that we were able to compensate for the gravitational sag by varying the stringing tensions of the stereo angle wires throughout the sector.

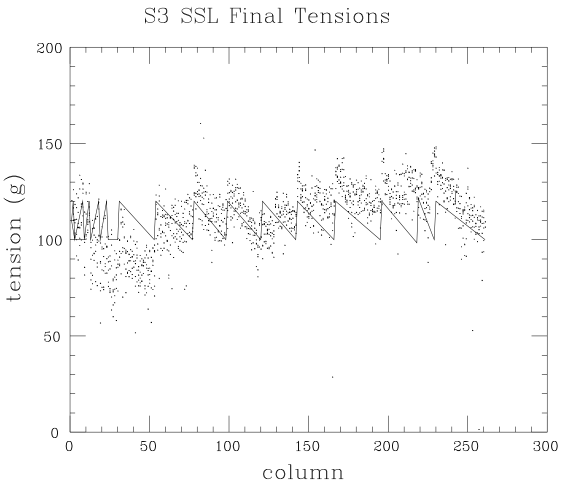

Figure 16: The final tensions on the field and guard wires of the sector 3 stereo super layer wires. The solid line shows the tensions that would be expected if the sag compensation scheme were correct. The sag compensation scheme used was based on measurements taken on sector 2 (Fig. 14), and that the final tensions do not lie near the solid line in the nose is indicative that the gravitational sag of sectors 2 and three is different.

Acknowledgements:

Ken Crane is given credit for realizing the effect of the gravitational sag of the sectors on the stereo angle wires.

All of the wire tension measurements reported in this document were made with a single wire tension monitor designed and constructed at Carnegie Mellon University.

References

[1] CEBAF Conceptual Design Report